Rigidity Transition in Materials: Hardness is Driven by Weak Atomic Constraints

Mathieu Bauchy,[1,*] Mohammad Javad Abdolhosseini Qomi,[2] Christophe Bichara,[3] Franz-Josef Ulm,[2,4] and Roland J.-M. Pellenq[2,3,4]

[1]*Department of Civil and Environmental Engineering, University of California, Los Angeles, California 90095, USA*
[2]*Concrete Sustainability Hub, Department of Civil and Environmental Engineering, Massachusetts Institute of Technology, 77 Massachusetts Avenue, Cambridge, Massachusetts 02139, USA*
[3]*Centre Interdisciplinaire des Nanosciences de Marseille, CNRS and Aix-Marseille University, Campus de Luminy, Marseille, 13288 Cedex 09, France*
[4]*MIT-CNRS joint laboratory at Massachusetts Institute of Technology, 77 Massachusetts Avenue, Cambridge, Massachusetts 02139, USA*

(Received 27 August 2014; published 23 March 2015)

Understanding the composition dependence of the hardness in materials is of primary importance for infrastructures and handled devices. Stimulated by the need for stronger protective screens, topological constraint theory has recently been used to predict the hardness in glasses. Herein, we report that the concept of rigidity transition can be extended to a broader range of materials than just glass. We show that hardness depends linearly on the number of angular constraints, which, compared to radial interactions, constitute the weaker ones acting between the atoms. This leads to a predictive model for hardness, generally applicable to any crystalline or glassy material.

DOI: 10.1103/PhysRevLett.114.125502 PACS numbers: 62.20.Qp, 31.15.xv, 61.43.−j

Rigidity theory [1–4], or topological constraint theory, is a powerful tool for capturing the atomic topology of glasses by reducing their network to mechanical trusses [5]. Following this mechanical analogy, a glass can be flexible, stressed–rigid, or isostatic, if the number of constraints per atom n_c, comprising radial bond stretching (BS) and angular bond bending (BB), is lower, higher, or equal to three, the number of degrees of freedom per atom, respectively. Flexible networks show internal degrees of freedom, the floppy modes [6], which allow for local deformations; whereas stressed–rigid ones are completely locked by their high connectivity. In between, by being rigid but free of eigenstress [7], compositions exhibiting an isostatic behavior show some remarkable properties, such as a space-filling tendency [8], very weak aging [9], and anomalous behaviors, such as maximal fracture toughness [10].

One of the major successes of this approach is the design of the Gorilla© Glass 3 by Corning©, which was created by atomic-scale modeling before anything had been melted in the lab [11,12]. Indeed, by capturing the chemical details of glasses that are relevant to macroscopic properties while filtering out those that are not, rigidity theory [13–15] has been used to predict the composition dependence of hardness, H, which characterizes resistance to permanent deformations under a load. Hence, topological constraint theory is a promising tool for designing stronger materials, which has recently been identified as a "grand challenge" for the future [16–18]. Topological constraint theory has also been applied to studying the folding of proteins [19,20]. However, it is still unknown whether it could be applied to a larger range of materials and, consequently, used to predict mechanical properties like hardness from the mere knowledge of composition.

Recently, relying on molecular dynamics (MD) simulations, we showed that rigidity concepts could be applied to calcium-silicate-hydrate, $(CaO)_x(SiO_2)_{1-x-y}(H_2O)_y$, or C-S-H, the binding phase of concrete [21]. From a topological point of view, C-S-H is a complex material as (1) it contains several chemical components, (2) its structure is anisotropic, inhomogeneous, and partially crystalline [22–27], and (3) in contrast to chalcogenide glass for which all bonds and angles are intact, it features some thermally broken constraints [21]. This provides motivation to extend the rigidity analysis of C-S-H to a broad range of compositions. We find that C-S-H undergoes a rigidity transition with respect to its composition. We show that hardness does not depend on the total number of constraints in the network, but only on the weaker ones, related to angular bond bending. On this basis, we propose a model for predicting hardness that demonstrates good results for different families of materials.

The molecular samples of C-S-H with different compositions were obtained by introducing defects in an 11 Å tobermorite configuration [28]. The C-S-H structures consist of defective calcium-silicate sheets, separated from each other by an interlayer spacing, which contains interlayer water molecules, hydroxyl groups, and charge-balancing calcium cations. The procedure used to prepare the samples and validations against a broad range of experimental values can be found in [29] and in the Supplemental Material [30].

To apply the topological constraint analysis to C-S-H, we relied on MD simulations of 150 samples of various

compositions, the main order parameter being the Ca/Si atomic ratio. Following the methodology reported in Ref. [21], we analyzed each MD trajectory to enumerate BS and BB constraints using a method already well established for chalcogenide and oxide glasses [35–39]. To count the number of BS constraints that apply to a central atom, we compute the radial excursion σ_r of each neighbor. A low σ_r is associated with an active BS constraint, whereas a high σ_r comes from the absence of an underlying constraint that would maintain the bond length fixed around its average value. We perform the same kind of analysis to enumerate the BB constraints applying to a central atom 0 by computing the angular excursion σ_θ of each angle $i\hat{0}j$ formed with the i, j first neighbors. Following this method, the distinction between active and inactive constraints can be clearly established at the atomic scale [21,38]. Note that free water molecules are excluded from this enumeration, as they do not belong to the network and, thus, do not contribute to its global rigidity. Hence, the method allows obtaining $n_c = n_{\mathrm{BS}} + n_{\mathrm{BB}}$ by only relying on MD.

As shown in Fig. 1, n_c decreases with Ca/Si, effectively separating a stressed-rigid domain from a flexible one. Specifically, C-S-H shows a rigidity transition according to composition, from flexible ($n_c < 3$) at a high Ca/Si ratio, to stressed-rigid ($n_c > 3$) at a low Ca/Si ratio, and an isostatic behavior ($n_c = 3$) at Ca/Si $\simeq 1.5$. This result constitutes the first direct evidence of a rigidity transition in a nonglassy material. It is worth noticing that the Ca/Si $\simeq 1.5$ transition composition also corresponds to structural and mechanical transitions. Indeed, the system is crystalline and transversely isotropic at low Ca/Si ratios, and amorphous and isotropic at high Ca/Si ratios [29]. This feature is very similar to what is typically observed in glasses, since stressed-rigid compositions show a weak glass-forming ability and tend to easily crystalize [4]. In addition, the change of slope of n_c at Ca/Si $\simeq 1.5$ appears to arise from the onefold coordinated H atoms, which typically stiffen (soften) flexible (stressed-rigid) networks [40].

For glasses showing such a composition-driven rigidity transition, like Ge-Se, hardness typically shows a linear correlation with the average coordination number $\bar{r}$ [10] and, therefore, to n_c, which is usually given by $n_c = 5\bar{r}/2 - 3$, when all BS and BB constraints are active. Following this observation, an attempt to predict the hardness of oxide glasses via topological constraint theory has been proposed by Smedskjaer and Mauro [13,14]. This model relies on the following assumptions: (1) a network requires a minimum number of constraints per atom $n_c = n_{\mathrm{crit}}$ to be cohesive, i.e., for H to be nonzero; (2) each additional constraint n_c-n_{crit} then contributes to increasing H. This leads to

$$H = (dH/dn_c)[n_c - n_{\mathrm{crit}}], \tag{1}$$

where (dH/dn_c) is a parameter determined empirically and n_{crit} was found to be equal to 2.5. Predicted H values were found to show a good agreement with experimental data for several borate glasses [13,14].

To check the applicability of Mauro's model to more complex materials like C-S-H, we computed H for each of the 150 simulated samples. The details of the calculation and the validation versus experiments can be found in Ref. [29] as well as in the Supplemental Material [30]. Figure 2 shows H with respect to the Ca/Si molar ratio. Overall, H follows the same trend as n_c, namely, a

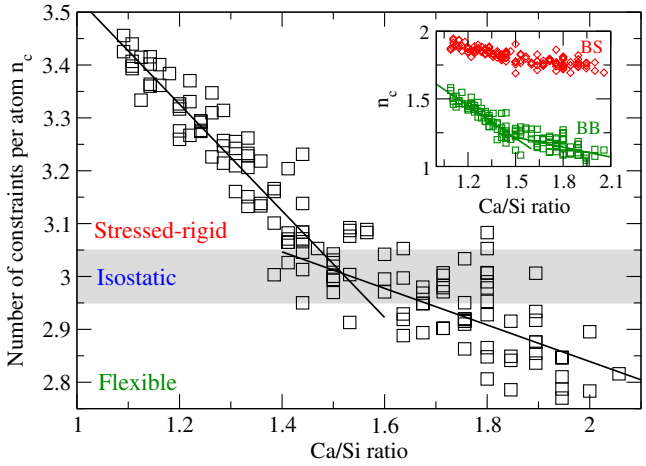

FIG. 1 (color online). Number of constraints per atom n_c as a function of the Ca/Si molar ratio. The inset shows the contributions of the radial (BS) and angular (BB) constraints. Lines are linear fits in flexible and stressed-rigid domains and serve as guides for the eye.

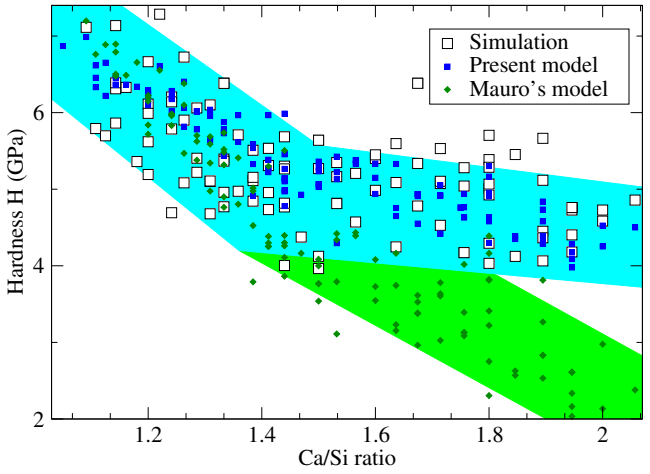

FIG. 2 (color online). Computed hardness of C-S-H (white squares) [29] and comparison with the values predicted by Mauro's model (green diamonds) using Eq. (1), and by the present model using Eq. (2). Colored areas are guides for the eye, to distinguish the predictions of the two models in the Ca/Si > 1.5 domain.

continuous decrease with Ca/Si, with a change of slope around Ca/Si = 1.5, which suggests that H and n_c are, indeed, correlated. The (dH/dn_c) and n_{crit} parameters of Mauro's model were then obtained by fitting the computed H values with respect to n_c. Note that Ca/Si is not the only order parameter of the system; the fraction of adsorbed water can also change for the different sample, so that n_c and, consequently, the predicted values of hardness do not depend only on Ca/Si. As can be seen in Fig. 2, Mauro's model fails to describe the dependence of H over the full range of composition as it cannot predict the two different slopes in the flexible and stressed-rigid domains, respectively. This can be explained by the fact that Mauro's model assumes an equivalent contribution of each constraint to the macroscopic hardness. However, the energy of BB constraints is typically lower than that of BS constraints [38,41], so that both should not necessarily contribute with the same weight to hardness. Moreover, angular and radial constraints should have a different contribution to resist different kinds of deformations like bulk isostatic compression or shearing. As hardness has been shown to be closely correlated to the resistance to shear [42], we propose that H should depend mostly on the number of angular BB constraints per atom n_{BB}. This leads to a modified model for hardness prediction of the form

$$H = (dH/dn_{\mathrm{BB}})[n_{\mathrm{BB}} - n_{\mathrm{BB}}^{\mathrm{crit}}], \tag{2}$$

where (dH/dn_{BB}) and $n_{\mathrm{BB}}^{\mathrm{crit}}$ are empirically determined parameters. This assumption is justified by the fact that, during hardness measurements, the network rearrangements, occurring around the tip of the indenter, should follow the lowest energy paths; i.e., they should preferably involve breakings or reformations of BB constraints, with energy that is lower than that of BS constraints. In other words, hardness should be driven only by the weaker atomic constraints. As shown in Fig. 2, this new model provides a more accurate prediction of H over the full composition range for C-S-H.

The correlation between H and n_{BB} for C-S-H can now be used as a predictive tool. Relying on the MD-based constraints enumeration in C-S-H, we identified the average number of constraints created by each element over the studied range of compositions. The results are reported in Table I. As expected and observed in silicate glasses [38],

TABLE I. Enumeration of BS and BB constraints created by each element. Note that BS constraints have been fully attributed to the cations.

Atom	Composition	BS	BB	BS+BB
Si	1-x-y	4	5	9
Ca	x	5	0	5
H	2y	1	0	1
O	2-x-y	⋯	1	1
Total	3-x			

Si atoms are characterized by 4 BS and 5 BB constraints. H atoms show only 1 BS constraint with their nearest O neighbor [43]. On average, Ca atoms undergo 5 BS constraints. This highlights the fact that the effective number of active BS constraints can differ from the coordination number, as also reported for Na atoms in silicate glasses [38]. As opposed to covalent Si-O bonds, Ca-O bonds are more ionic and nondirectional, so that Ca atoms do not show any BB constraints [21]. On average, each O atom shows 1 active BB constraint. Note that O atoms can show different environments in the system (bridging or nonbridging oxygen in the silicate network, and hydroxyl groups attached to Ca atoms between the layers), which makes it challenging to evaluate the number of BS constraints they undergo. For greater convenience, every BS constraint created between O and Si, H, or Ca atoms have, thus, been fully attributed to the corresponding cation. Hence, this enumeration permits us to calculate analytically n_{BS}, n_{BB}, and n_c for any stoichiometry (x, y), where x and y are the molar fraction of calcium oxide and reacted structural water, respectively. This leads to $n_c = (11-5x-8y)/(3-x)$ and $n_{\mathrm{BB}} = (7-6x+6y)/(3-x)$, which allows calculating $H(x, y)$ with our model. The resulting prediction is shown in Fig. 3. More generally, with the knowledge of $n_c(x, y)$, one can now build a ternary rigidity phase diagram of C-S-H. As shown in Fig. 3, C-S-H features three domains: (1) likely noncohesive at high water content, when $n_c < 2.5$ [13], (2) stressed rigid at high silica content, and (3) flexible in between. The boundary between the flexible and stressed–rigid domains, the optimal isostatic compositions, are obtained for $n_c = 3$, i.e., for $4y + x = 1$.

We now aim to check the extent of applicability of our model, i.e., if hardness linearly depends on the number of bond-bending constraints for other materials, for which both H and n_{BB} are known. Note that Mauro's model and the present one are equivalent if n_{BS} and n_{BB} are linearly dependent on each other, which is the case when all angles are constrained, so that $n_{\mathrm{BB}} = 4n_{\mathrm{BS}} - 3$. This usually holds for chalcogenide glasses, but not for silicate and borate glasses, which feature ionic and nondirectional bonds like Ca-O and Na-O [38]. First, glassy silica (g-SiO_2) and crystalline quartz (c-SiO_2) are natural choices to check to what extent the predictions, based on the model developed for C-S-H, can be extrapolated to different compositions. Although they show a similar coordination (fourfold Si and twofold O atoms), glassy silica differs from quartz by a broader Si-O-Si angular distribution [37,44,45], such that the constraint associated to this angle is considered broken in glassy silica and intact in quartz [37,44]. This leads to $n_{\mathrm{BB}} = 1.67$ and 2.33 for g-SiO_2 and c-SiO_2, respectively. As shown in Fig. 4, experimental H values show a linear dependence on n_{BB}, which is in agreement with our model, although the large experimental error bars prevent us from being more conclusive. Second, H values obtained by

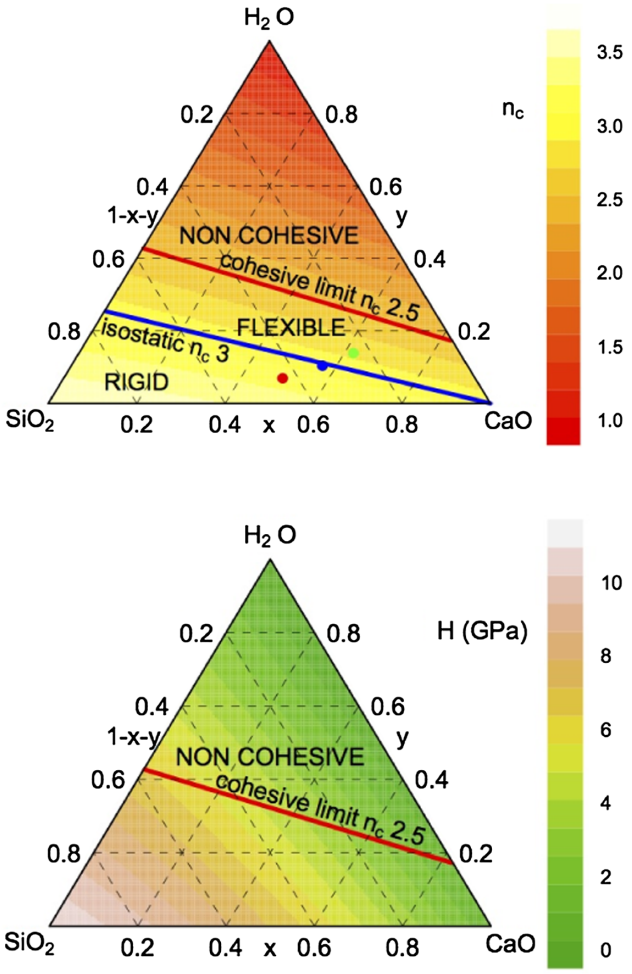

FIG. 3 (color online). Predictions of the number of constraints per atom (top) and of the hardness (bottom) as a function of the composition of C-S-H. The red and blue lines are respective predictions of the cohesive limit of the system and of the isostatic compositions. The green, blue, and red points in the top figure represent the compositions of three selected computed samples being, respectively, flexible, isostatic, and rigid.

Mauro *et al.* [13] for soda lime borate glasses, and used as a basis to develop Eq. (1), were plotted versus n_{BB} instead of versus n_c in the original work. As shown in Fig. 4, a fairly linear trend is found, which supports the present model. Note that, in the original work, the presence of some additional modifier rigidity, due to clustering effects, was assumed in order to obtain a linear relationship between H and n_c [13]. This assumption is not needed any more in our model. Third, as expected, and shown in Fig. 4, the present model is also valid for chalcogenide glasses. Hence, we note that, for several different families of materials, hardness is closely correlated to n_{BB}, the number of angular constraints. This highlights the importance of controlling the number of weak BB constraints when designing new materials from the atomic scale. In return, the parameters of the present model (dH/dn_{BB}) and $n_{\mathrm{BB}}^{\mathrm{crit}}$ appear to be material specific and not universal.

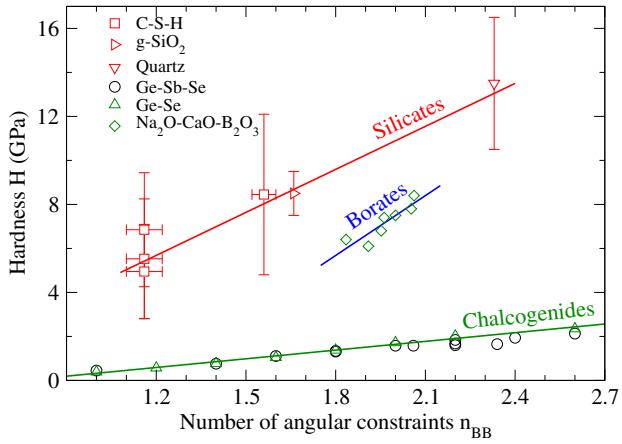

FIG. 4 (color online). Experimental values of the hardness of C-S-H (squares) [29], glassy silica (right triangle) [46], quartz (bottom triangle) [46], soda-lime-borates glasses (diamonds) [13], Ge-Se glasses (up triangles) [47], and Ge-Sb-Se (circles) [48] as a function of the number of angular constraints per atom. Fitting parameters are $(dH/dn_{\mathrm{BB}}) = 6.5, 9.1, 1.3$ (which appear to scale with the bond energy, i.e., $\mathrm{B-O} > \mathrm{Si-O}/\mathrm{Ca-O} > \mathrm{Ge-Se}$) and $n_{\mathrm{BB}}^{\mathrm{crit}} = 0.33,\ 1.2,\ 0.75$ for silicates, borates, and chalcogenides, respectively. Lines are guides for the eye.

Hence, the original Phillips' topological constraint theory, which assumes that all constraints are equivalent, cannot resolve mechanical properties. Indeed, as shown here, BS and BB constraints contribute differently to the hardness. We expect that the low energy BB constraints, which provide modes of deformation associated to lower activation energy, also play a critical role in the aging of materials. This model has been applied to silicate, borate, and chalcogenide materials, which all feature weak BB constraints. However, for other families of materials, a better knowledge of the relative strength of each constraint would allow identifying the weaker ones, which will likely contribute to the macroscopic hardness.

Overall, these results suggest that rigidity concepts can be extended to a broader range of materials than just glasses. By capturing the important atomic topology while getting rid of the chemical details that ultimately do not affect macroscopic properties, topological constraint theory has the potential to be used as an effective predictive tool to optimize well developed materials, such as ordinary Portland cement. For example, we can expect isostatic C-S-H compositions, around $\mathrm{Ca/Si} = 1.5$, to show the usual properties of isostatic glasses, such as maximal fracture toughness and very weak aging phenomena [49,50].

This work has been carried out within the framework of the ICoME2 Labex (ANR-11-LABX-0053) and the A*MIDEX projects (ANR-11-IDEX-0001-02) cofunded by the French program "Investissements d'Avenir" which is managed by the ANR, the French National Research Agency.

*bauchy@ucla.edu; http://mathieu.bauchy.com

[1] J. C. Phillips, J. Non-Cryst. Solids **34**, 153 (1979).
[2] J. C. Phillips, J. Non-Cryst. Solids **43**, 37 (1981).
[3] M. F. Thorpe, J. Non-Cryst. Solids **57**, 355 (1983).
[4] J. C. Mauro, Am. Ceram. Soc. Bull. **90**, 31 (2011).
[5] J. C. Maxwell, Philos. Mag. **27**, 294 (1864).
[6] G. G. Naumis, Phys. Rev. E **71**, 026114 (2005).
[7] M. V. Chubynsky, M. A. Briere, and N. Mousseau, Phys. Rev. E **74**, 016116 (2006).
[8] K. Rompicharla, D. I. Novita, P. Chen, P. Boolchand, M. Micoulaut, and W. Huff, J. Phys. Condens. Matter **20**, 202101 (2008).
[9] S. Chakravarty, D. G. Georgiev, P. Boolchand, and M. Micoulaut, J. Phys. Condens. Matter **17**, L1 (2005).
[10] A. K. Varshneya and D. J. Mauro, J. Non-Cryst. Solids **353**, 1291 (2007).
[11] J. C. Mauro, A. J. Ellison, and L. D. Pye, Int. J. Appl. Glass Sci. **4**, 64 (2013).
[12] J. C. Mauro and M. M. Smedskjaer, Physica A (Amsterdam) **391**, 6121 (2012).
[13] M. M. Smedskjaer, J. C. Mauro, and Y. Yue, Phys. Rev. Lett. **105**, 115503 (2010).
[14] M. M. Smedskjaer, J. C. Mauro, S. Sen, J. Deubener, and Y. Yue, J. Chem. Phys. **133**, 154509 (2010).
[15] M. M. Smedskjaer, Front. Mater. **1**, 23 (2014).
[16] J. C. Mauro and E. D. Zanotto, Int. J. Appl. Glass Sci. **5**, 313 (2014).
[17] J. C. Mauro, C. S. Philip, D. J. Vaughn, and M. S. Pambianchi, Int. J. Appl. Glass Sci. **5**, 2 (2014).
[18] J. C. Mauro, Front. Mater. **1**, 20 (2014).
[19] A. J. Rader, B. M. Hespenheide, L. A. Kuhn, and M. F. Thorpe, Proc. Natl. Acad. Sci. U.S.A. **99**, 3540 (2002).
[20] J. C. Phillips, J. Phys. Condens. Matter **16**, S5065 (2004).
[21] M. Bauchy, M. J. Abdolhosseini Qomi, C. Bichara, F.-J. Ulm, and R. J.-M. Pellenq, J. Phys. Chem. C **118**, 12485 (2014).
[22] R. J.-M. Pellenq, A. Kushima, R. Shahsavari, K. J. V. Vliet, M. J. Buehler, S. Yip, and F.-J. Ulm, Proc. Natl. Acad. Sci. U.S.A. **106**, 16102 (2009).
[23] H. Manzano, S. Moeini, F. Marinelli, A. C. T. van Duin, F.-J. Ulm, and R. J.-M. Pellenq, J. Am. Chem. Soc. **134**, 2208 (2012).
[24] M. J. Abdolhosseini Qomi, M. Bauchy, R. J.-M. Pellenq, and F.-J. Ulm, in *Mechanics and Physics of Creep, Shrinkage, and Durability of Concrete: A Tribute to Zdenek P. Bazant: Proceedings of the Ninth International Conference on Creep, Shrinkage, and Durability Mechanics (CONCREEP-9), September 22-25, 2013 Cambridge, Massachusetts* (ASCE Publications, Reston, VA, 2013), pp. 78–85.
[25] M. Bauchy, M. J. Abdolhosseini Qomi, F.-J. Ulm, and R. J.-M. Pellenq, J. Chem. Phys. **140**, 214503 (2014).
[26] M. J. Abdolhosseini Qomi, F.-J. Ulm, and R. J.-M. Pellenq, J. Am. Ceram. Soc. **95**, 1128 (2012).
[27] M. J. Abdolhosseini Qomi, M. Bauchy, F.-J. Ulm, and R. J.-M. Pellenq, J. Chem. Phys. **140**, 054515 (2014).
[28] S. Hamid, Z. Kristallogr. **154**, 189 (1981).
[29] M. J. Abdolhosseini Qomi, K. J. Krakowiak, M. Bauchy, K. L. Stewart, R. Shahsavari, D. Jagannathan, D. B. Brommer, A. Baronnet, M. J. Buehler, S. Yip, F.-J. Ulm, K. J. Van Vliet, and R. J.-M. Pellenq, Nat. Commun. **5**, 4960 (2014).
[30] See Supplemental Material at http://link.aps.org/supplemental/10.1103/PhysRevLett.114.125502 for a description of simulation methods and hardness computation, which includes Refs. [31–34].
[31] R. Shahsavari, R. J.-M. Pellenq, and F.-J. Ulm, Phys. Chem. Chem. Phys. **13**, 1002 (2011).
[32] M. Bauchy, M. J. Abdolhosseini Qomi, R. J. M. Pellenq, and F. J. Ulm, in *Computational Modelling of Concrete Structures: Proceedings of EURO-C 2014, St. Anton am Arlberg, Austria, 24-27 March 2014* (CRC Press, Boca Raton, 2014), p. 169.
[33] S. Soyer-Uzun, S. R. Chae, C. J. Benmore, H.-R. Wenk, and P. J. M. Monteiro, J. Am. Ceram. Soc. **95**, 793 (2012).
[34] F. P. Ganneau, G. Constantinides, and F. J. Ulm, Int. J. Solids Struct. **43**, 1727 (2006).
[35] M. Micoulaut, J. Raty, C. Otjacques, and C. Bichara, Phys. Rev. B **81**, 174206 (2010).
[36] M. Bauchy, Am. Ceram. Soc. Bull. **91**, 34 (2012).
[37] M. Bauchy, M. Micoulaut, M. Celino, S. Le Roux, M. Boero, and C. Massobrio, Phys. Rev. B **84**, 054201 (2011).
[38] M. Bauchy and M. Micoulaut, J. Non-Cryst. Solids **357**, 2530 (2011).
[39] M. Bauchy and M. Micoulaut, Phys. Rev. Lett. **110**, 095501 (2013).
[40] P. Boolchand, M. Zhang, and B. Goodman, Phys. Rev. B **53**, 11488 (1996).
[41] P. K. Gupta and J. C. Mauro, J. Chem. Phys. **130**, 094503 (2009).
[42] X. Jiang, J. Zhao, and X. Jiang, Comput. Mater. Sci. **50**, 2287 (2011).
[43] P. Boolchand and M. F. Thorpe, Phys. Rev. B **50**, 10366 (1994).
[44] M. Zhang and P. Boolchand, Science **266**, 1355 (1994).
[45] H. F. Poulsen, J. Neuefeind, H. B. Neumann, J. R. Schneider, and M. D. Zeidler, J. Non-Cryst. Solids **188**, 63 (1995).
[46] W. C. Oliver and G. M. Pharr, J. Mater. Res. **7**, 1564 (1992).
[47] J.-P. Guin, T. Rouxel, J.-C. Sanglebœuf, I. Melscoët, and J. Lucas, J. Am. Ceram. Soc. **85**, 1545 (2002).
[48] D. Swiler, A. K. Varshneya, and R. Callahan, J. Non-Cryst. Solids **125**, 250 (1990).
[49] M. Bauchy, H. Laubie, M. J. A. Qomi, C. G. Hoover, F.-J. Ulm, and R. J.-M. Pellenq, arXiv:1410.2915.
[50] M. Bauchy, M. J. A. Qomi, C. Bichara, F.-J. Ulm, and R. J.-M. Pellenq, arXiv:1410.2916.